



**HAL**  
open science

# Long-range alteration of the physical environment mediates cooperation between *Pseudomonas aeruginosa* swarming colonies

Maxime Deforet

► **To cite this version:**

Maxime Deforet. Long-range alteration of the physical environment mediates cooperation between *Pseudomonas aeruginosa* swarming colonies. *Environmental Microbiology*, 2023, 10.1101/2022.06.29.498166 . hal-03867846

**HAL Id: hal-03867846**

**<https://hal.science/hal-03867846>**

Submitted on 23 Nov 2022

**HAL** is a multi-disciplinary open access archive for the deposit and dissemination of scientific research documents, whether they are published or not. The documents may come from teaching and research institutions in France or abroad, or from public or private research centers.

L'archive ouverte pluridisciplinaire **HAL**, est destinée au dépôt et à la diffusion de documents scientifiques de niveau recherche, publiés ou non, émanant des établissements d'enseignement et de recherche français ou étrangers, des laboratoires publics ou privés.

1 Long-range alteration of the physical environment mediates  
2 cooperation between *Pseudomonas aeruginosa* swarming  
3 colonies

4 Maxime Deforet<sup>1,\*</sup>

5 1. Sorbonne Université, Centre National de la Recherche Scientifique, Laboratoire Jean Perrin,  
6 LJP, Paris 75005, France;

7 \* E-mail: maxime.deforet@sorbonne-universite.fr.

8 *Keywords: Pseudomonas aeruginosa, swarming, agar gel, surfactants, rhamnolipids.*

9

## Abstract

10 *Pseudomonas aeruginosa* makes and secretes massive amounts of rhamnolipid surfactants that en-  
11 able swarming motility over biogel surfaces. But how this rhamnolipids interact with biogels to  
12 assist swarming remains unclear. Here I use a combination of optical techniques across scales  
13 and genetically-engineered strains to demonstrate that rhamnolipids can induce agar gel swelling  
14 over distances  $>10,000\times$  the body size of an individual cell. The swelling front is on the micro-  
15 metric scale, and is easily visible using shadowgraphy. Rhamnolipid transport is not restricted  
16 to the surface of the gel, but occurs through the whole thickness of the plate and, consequently,  
17 the spreading dynamics depends on the local thickness. Surprisingly, rhamnolipids can cross the  
18 whole gel and induce swelling on the opposite side of a two-face Petri dish. The swelling front  
19 delimits an area where the mechanical properties of the surface properties are modified: wa-  
20 ter wets the surface more easily, which increases the motility of individual bacteria and enables  
21 collective motility. A genetically-engineered mutant unable to secrete rhamnolipids (*rhlA*<sup>-</sup>), and  
22 therefore unable to swarm, is rescued from afar with rhamnolipids produced by a remote colony.  
23 These results exemplify the remarkable capacity of bacteria to change the physical environment  
24 around them and its ecological consequences.

25

## Introduction

26 Bacteria have a remarkable ability to change the world around them through their collective  
27 behaviors [1, 2, 3]. Some of these changes are physical : bacteria interact mechanically with their  
28 environment [4] and they are also able to feedback on the physical environment [5, 6, 7].

29 Petri dishes with an agar biogel are widely used to investigate collective bacterial motility and  
30 its interplay with other biological processes [8]. This approach was used to uncover chemotactic  
31 genes [9, 10], mechanisms of action of pharmaceutical molecules [11], evolutionary dynamics  
32 [12], quorum sensing [13, 14], and other social behaviors of bacteria [15, 16, 17].

33 Agar gel serves as a physical and chemical substrate: cells are inoculated at the surface of the  
34 gel, they proliferate by consuming essential nutrients supplemented to the gel. In that regard, an

35 agar plate is generally viewed as a passive element merely providing mechanical support, water,  
36 and nutrients. During colony growth, bacteria secrete osmolytes (exopolysaccharides), which  
37 draw water from the gel to equilibrate osmotic imbalance and contribute to colony swelling and  
38 expansion, in non-motile [18, 19] as well as in motile colonies [20, 21, 22]. While colony morpho-  
39 genesis modeling attempts sometimes include nutrient and water depletion [23, 24], structural  
40 changes of agar gel are rarely considered.

41 In the case of the bacterium *Pseudomonas aeruginosa*, a common opportunistic pathogen, an-  
42 other gel modification needs to be considered: *P. aeruginosa* secretes rhamnolipids, a family of  
43 glycolipid surfactants of strong interest in medicine [25] and industry [26, 27], in particular for  
44 their antimicrobial properties, their capacity to emulsify oil and participate in bioremediation,  
45 and their good environmental compatibility and biodegradability. Secretion of rhamnolipids al-  
46 lows the colony to rapidly and collectively spread into a branched shape, a phenotype called  
47 swarming [28, 29]. Mutants that do not secrete rhamnolipids are unable to swarm [30, 31]. Due  
48 to their surfactant nature [32], rhamnolipids are often said to *lubricate the surface* [33], decrease  
49 *friction against the gel* [34], *act as a wetting agent* [35], or *lower surface tension* [20, 36]. But how the  
50 rhamnolipids interact with the agar biogel to enable swarming motility remains unclear.

51 Previous work used biophysical approaches to study how surfactant-assisted spreading of  
52 liquid film can yield to branching. This has been explored on liquid and solid substrates [37, 38],  
53 and was extended to the case of *P. aeruginosa* swarming colonies [39, 40]. In those works, rham-  
54 nolipids were modeled as a thin film of insoluble surfactants secreted by the colony and diffusing  
55 at the surface of a gel. Differences of surfactant concentration inside and outside the colony yield  
56 to gradients of surface tension and induced a branching instability (Marangoni effect). These  
57 modeling efforts ignored what was happening on the colony side, where a precursor film was  
58 sometimes observed. In particular, rhamnolipids are soluble in water [41] and these molecules  
59 are substantially smaller than the agar gel pores. Therefore, they are expected to diffuse though  
60 the entire agar gel, a hydrogel, whose structure can be modified through swelling [42, 43]. Bulk  
61 effects might complement surface effects and alter colony morphogenesis.

62 Here, I use a combination of imaging methods across scales to demonstrate that rhamnolipids

63 secreted by the colony alter the physical properties of the agar gel, not only locally where they  
64 are secreted, but also all more widely around the bacteria. Moreover, their transport is not  
65 restricted to the surface. I find, instead, that the rhamnolipids imbibe the whole gel, which yields  
66 to gel swelling with a sharp swelling front. Bulk transport of rhamnolipids directly affects the  
67 expansion rate of the region imbibed by rhamnolipids. Gel imbibition by rhamnolipids cover so  
68 large distances that rhamnolipid-deficient colonies can be remotely rescued. More generally, this  
69 is an example of the remarkable ability of bacteria to change the mechanical properties of the  
70 world surrounding them.

## 71 **Methods**

### 72 *Bacterial strains and growth conditions*

73 The bacterial strains used in this study are described in Table S1. Bacterial cells were routinely  
74 grown in LB at 37°C with aeration. Swarming plates were prepared as previously described [31].  
75 Agar concentration, unless specified otherwise, is 0.5 % (w/v). Overnight culture of bacteria were  
76 washed twice in PBS and 2 µL of the washed suspension were used to inoculate a swarming plate  
77 in the center. The plates were then flipped and placed inside a 37°C microbiological incubator.  
78 *rhlA*<sup>-</sup> *pBAD-RhlAB* colonies were grown on 1% L-arabinose swarming plates to induce expression  
79 of the *rhlA* gene and robust secretion of rhamnolipids.

### 80 *Whole swarming colony*

81 An automated device was built inside a microbiological incubator (Heratherm IGS 100, Ther-  
82 moFisher Scientific), for fluorescence, shadowgraphy, and brightfield imaging of a 10-cm diameter  
83 Petri dish. A LED light source (pE-4000, Cooled, UK) was used for fluorescence excitation. A set  
84 of lenses and mirrors were used to bring an even illumination pattern onto the plate. A single  
85 LED light source (Thorlabs, USA) was positioned on one side of the chamber for shadowgraphy  
86 imaging. Generic white LED strings (Mouser, France) were positioned above the plate for bright-  
87 field imaging. Images were acquired with a CMOS camera (Cellcam Centro, Cairn Research,

88 UK) with a macro lens (Navitar MVL7000, Thorlabs, USA). A dual-band emission filter (59010m,  
89 Chroma, USA) was mounted between the camera and the lens, for green and red fluorescence  
90 imaging. All devices were controlled with  $\mu$ Manager (<http://www.micro-manager.org>).

### 91 *Sessile droplets*

92 Plates and swarming colonies were prepared as explained above. Plates were taken out of the  
93 incubator and placed under a Axiozoom V16 microscope (Zeiss), set at the lowest magnification  
94 (field of view is 25.7x21.5mm), equipped with a CMOS camera (BlackFly S, FLIR, USA), and  
95 illuminated through a transilluminator (Zeiss) with a mirror position that mimics DIC illumi-  
96 nation. 1  $\mu$ L droplets of swarming media (recipe identical to that of the swarming plate, but  
97 without agar) were deposited on the surface of the gel, either inside or outside the swelling front  
98 generated by the colony. A movie was recorded as tens of droplets were deposited. Footprint  
99 diameters were measured, immediately after deposition, using ImageJ.

### 100 *Fluorescent bead tracking*

101 For quantifying gel swelling, 1  $\mu$ m fluorescent polystyrene beads (F13083, ThermoFisher Scien-  
102 tific) were added during the swarming plate preparation (final concentration of  $10^5$  beads/mL).  
103 Colony were grown inside a microscopy incubator (Oko-Lab, Italy), mounted an a IX-81 Olym-  
104 pus inverted microscope, equipped with a LED light source (pE-4000, Cooled, UK). Images were  
105 taken with a 20x objective and a CMOS camera (BlackFly S, FLIR, USA), every minute, for 30  
106 minutes, while the swelling front was passing through the field of view (confirmed by phase-  
107 contrast imaging). Diffraction pattern detection, beads detection, tracking, and calculation of  
108 the vertical displacement were performed with custom-made routines in MATLAB (MathWorks,  
109 USA). Calibration between diffraction pattern radius and vertical position was done by taking a  
110 vertical stack of images.

111

## *Profilometry*

112 Height profiles were measured with a Zegage Pro interferometry profilometer (Zygo) equipped  
113 with a 5x Michelson objective (Nikon). An acquisition took 5 seconds (for one field of view 2x2.7  
114 mm), and 20 positions were stitched together to reconstruct the whole height profile (Figure 1E).  
115 For Figure 5C, the profiles were measured when the diameter of the rhamnolipids-imbibed area  
116 was approximately 3 cm in diameter. Four positions were recorded per plate (the 4th roots of  
117 unity). Each profile was then measured perpendicularly to the swelling front. The  $X = 0$  location  
118 was identified as the inflection point of the profile. The reference height  $Z = 0$  was imposed at  
119 location  $X = -500 \mu\text{m}$  and  $X = -400 \mu\text{m}$ , which tilt-corrected the whole profile. Heights in  
120 Figure 5C were measured at  $X = 1000 \mu\text{m}$ .

121

## *Stepwise substrate*

122 A 1.5 mm thick sheet of polydimethylsiloxane (PDMS) was made following standard protocol  
123 (RTV615A+B, 10:1, Momentive Performance Materials). A 1x2 cm slab was cut out of the PDMS  
124 sheet and was placed in a Petri dish. 20 mL of agar gel was then poured on top of the substrate,  
125 following usual swarming plate protocol.

126

## *Two-face Petri dish*

127 The bottom of a Petri dish was drilled with a 10-mm drill bit. Holes were deburred with a 13-mm  
128 drill bit. Dishes were sterilized in 70% ethanol. The bottom side of each hole was taped with a  
129 piece of Parafilm, which was peeled off after the agar gel was poured and solidified.

130

## *Single-cell motility*

131 A suspension of *rhlA*<sup>-</sup> cells growing in liquid swarming media was spun down. A 20  $\mu\text{L}$  plastic  
132 pipette tip was used to sample cells from the pellet and to transfer cells onto the gel surface  
133 (approximately 2 mm from the swelling front identified in shadowgraphy). One second videos  
134 (46 frames-per-second) were acquired every 5 minutes, at 10x magnification, in phase contrast,

135 with an IX-81 Olympus inverted microscope. Auto-focus was performed before each acquisition.  
136 Image analysis was performed independently for each video: Local density was measured on the  
137 first frame of the video, by thresholding the phase-contrast image, followed by local averaging.  
138 The Density Index, defined to be between 0 (no cell) and 1 (cells form a uniformly dark popu-  
139 lation) is therefore the proportion of neighboring pixels that contains cells. To evaluate motility,  
140 the difference between the maximum projection and the minimum projection across the time-  
141 stack yields to a map where pixels were bright if their grey values changed during the video.  
142 Then, a threshold was applied and the result was locally average to produce a map of Speed  
143 Index between 0 (no pixel change) and 1 (all pixels have change values). This coarse-grained  
144 quantification is valid as long as cells are not too dense and cells do not move too much during  
145 one video (therefore, the analysis was limited to the region of the field of view where cells did  
146 not pile up and only one-second long videos were considered). To check the robustness of the  
147 method, various thresholding values have been tried, without significantly affecting the results.

148

## Results

149

### *Rhamnolipids cause biogel swelling*

150 Wild-type *P. aeruginosa* colony spreads on soft agar by forming a branched colony, a behav-  
151 ior called swarming [29]. *rhlA*, a gene involved in production of rhamnolipids, is required for  
152 swarming: an *rhlA*<sup>-</sup> colony, which does not produce rhamnolipids, is unable to swarm (Figure  
153 1A). Shadowgraphy, an optical method that reveals non-uniformities in transparent media by  
154 casting a shadow onto a white background [44], revealed that an area of the gel around the  
155 rhamnolipid-producing colony was modified: a thin darker line surrounded the colony (Fig-  
156 ure 1B). Timelapse imaging confirmed this optical modification originated from the colony and  
157 propagates outward (See Movie S1). Since no modification emerged from an *rhlA*<sup>-</sup> colony, I hy-  
158 pothesized modification of the optical properties of the gel were due to secretion of rhamnolipids.

159 Rhamnolipids are secreted as a family of glycolipid molecules, made of one or two fatty  
160 acid chains (primarily 3-(3-hydroxyalkanoyloxy)alkanoic acid, HAA) associated with one or two

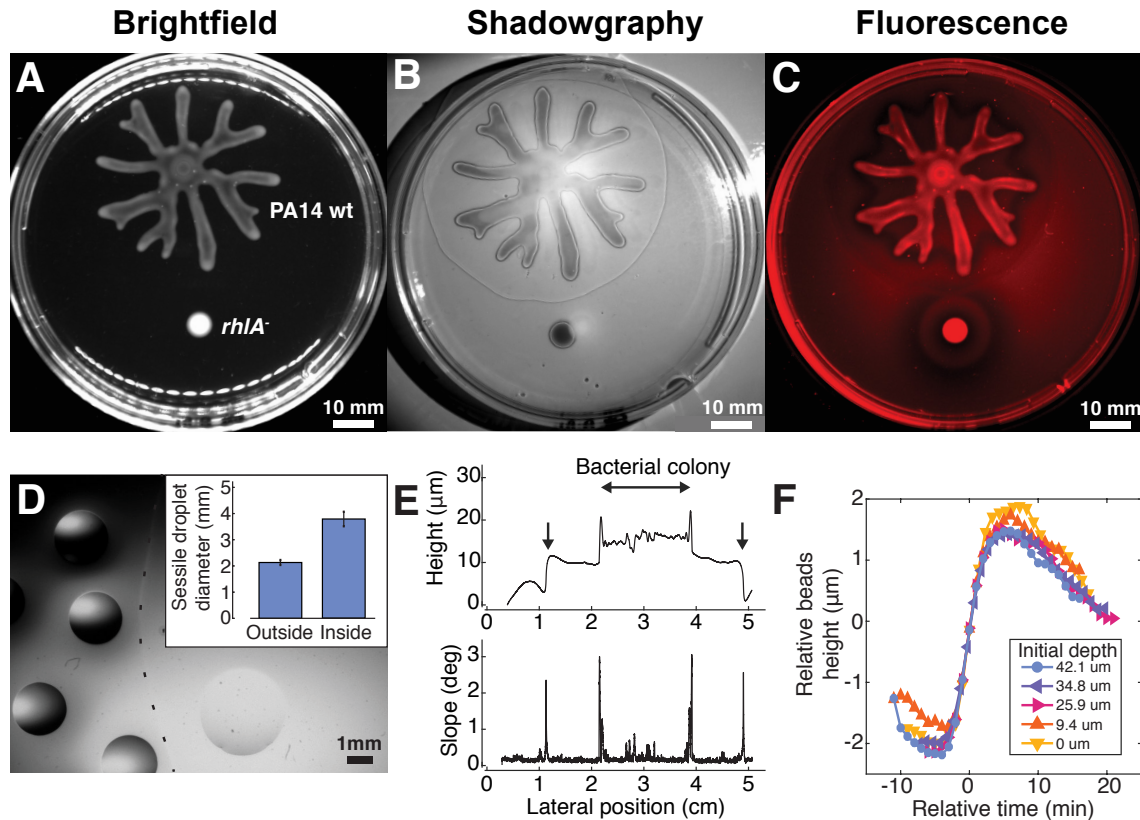


Figure 1: Rhamnolipids induce agar gel swelling. A-B-C: Wild-type *P. aeruginosa* and *rhIA*<sup>-</sup> colonies were grown on an agar gel. The former swarmed out and formed a branched colony, whereas the latter did not swarm. A: Brightfield image. B: Shadowgraphy image reveals a darker line (depicted by a black arrowhead) that corresponds to a swelling front. C: Fluorescence image, for Nile Red imaging, confirms the darker line corresponds to a boundary of an area imbued by rhamnolipids. D: An illustrative micrograph showing the sessile droplets experiments. Dashed line depicts the swelling front. The source colony is on the right side. Inset: comparison of the wetting footprint radius in the two conditions. Error bars are standard deviation. E: Top: a height profile of a gel, obtained from optical interferometry. Bottom: The local slope of the height profile. F: Vertical positions of fluorescent microbeads reveals gel swelling. The time axis for each trajectory is shifted using time synchronization from lateral displacement data (See Figure S1). Colors code for initial depth of each bead.

161 rhamnose groups, called monorhamnolipids (mono-RLs) or dirhamnolipids (di-RLs) [45]. These  
162 molecules are lipids, therefore they could be localized using a lipid dye. Nile Red, whose emis-  
163 sion spectrum depends on the polarity of the solvent [46], was mixed to the agar gel during gel  
164 preparation. Fluorescence microscopy confirmed a sharp drop of fluorescence intensity coincides  
165 with the location of the darker line visualized in shadowgraphy (Figure 1C). *rhlA*<sup>-</sup> colony does  
166 not produce HAA but still produces fatty acid chain precursors, whose lipid nature can be cap-  
167 tured by Nile Red imaging. In this case, fluorescence intensity gradually varied with the distance  
168 to the colony, but no sharp transition was observed. I also measured the wetting property of the  
169 gel surface by performing sessile droplets experiments [47]. Water droplets were deposited on  
170 each side of the darker line localized by shadowgraphy. On average, the droplet footprint radius  
171 was  $3.78 \pm 0.27$  (SD) mm on the colony side, and  $2.13 \pm 0.09$  (SD) mm on the other side (Figure  
172 1D). Neglecting gravity and therefore assuming a spherical cap shape allow the calculation of  
173 contact angles of  $22.7^\circ$  and  $35.6^\circ$ , respectively. The wetting footprint size was found to be uni-  
174 form on the colony side, independent of the distance to the colony or the distance to the darker  
175 line. Similarly, the wetting footprint size was found to be uniform also outside the darker line.  
176 This confirms that the darker line marks a sharp limit of the rhamnolipid range, with surface  
177 properties that correlates with the presence of rhamnolipids. (Of note, the resolution of the ses-  
178 sile droplet experiment does not enable to measure a gradient of surfactant concentration; the  
179 results merely demonstrate a contrast of concentration inside/outside the darker line.)

180 To understand the origin of the darker line visible in shadowgraphy, I had to first evaluate its  
181 3D profile. Using an optical profilometer (a device capable to measure 3D profile of a reflective  
182 surface with a nanometric resolution), I measured a jump of  $8 \mu\text{m}$ , with a maximal slope of  $3^\circ$   
183 (Figure 1E). The jump could emerge from two possible mechanisms: either it corresponds to a  
184 thick layer of rhamnolipid molecules covering the surface of the agar gel, as assumed by previous  
185 works [39, 40], or alternatively rhamnolipids infiltrate the gel and the jump corresponds to a gel  
186 swelling front. I embedded micrometric fluorescent beads during preparation of the gel and  
187 performed 3D-tracking to follow each bead while the line passed through the field of view. If  
188 rhamnolipids cover the gel surface, beads should not move. If rhamnolipids diffuse through

189 the gel and make it swell, beads should move up. Data shown in Figure 1F confirms a vertical  
190 movement of all the beads, synchronized with the passing line (see also Movie S2). The swelling  
191 amplitude was uniform across the first 50  $\mu\text{m}$  (optical limitations of fluorescence microscopy  
192 hamper deeper observations). Of note, beads also moved laterally with a similar amplitude: they  
193 first moved outwards and then inwards (this corresponds to a dilatation wave, see Figure S1 for  
194 more details). This confirms rhamnolipids make the agar gel swell over large distances, and the  
195 darker line corresponds to a swelling front that is so steep that it can be seen by a naked eye and  
196 by shadowgraphy.

### 197 *Rhamnolipids imbibe the bulk of the gel, not the surface*

198 If transport of rhamnolipids is restricted to the gel surface, or if rhamnolipids diffuse through  
199 the gel following normal diffusion, their spreading rate should not depend on the local thickness  
200 of the gel. On the contrary, if Darcy's law governs rhamnolipids' transport, their spreading dy-  
201 namics should depend on the local section of the gel. I used gels with varying thicknesses to test  
202 this hypothesis and check whether rhamnolipids imbibed the whole gel or only the upper part.  
203 First, I used gels with stepwise thickness. I placed a thick inert obstacle at the bottom surface of  
204 the Petri dish and poured the agar gel on top of them. The thickness of obstacles (1.5 mm) was  
205 chosen to be smaller than the gel thickness (3.5 mm) to make sure the upper surface remained  
206 flat. To simplify the geometry of the system and keep a local source of rhamnolipids, I inocu-  
207 lated a non-motile mutant (*flgK<sup>-</sup>*) along a line. The swelling front coming out of the colony was  
208 found to propagate faster on top of obstacles (Figure 2A), where the gel section was smaller, and  
209 slower on top of thicker sections of the gel, which is compatible with a transport of rhamnolipids  
210 through the whole gel. This effect was also found in gels of various thicknesses. Once again,  
211 thinner gels induced faster traveling speed of the swelling front (Figure 2B), in agreement with  
212 transport through the gel. Intriguingly, while thinner gels induce faster spreading of the swelling  
213 front, they also induce smaller swarming colonies (Figure S2). Finally, I tested the swelling speed  
214 in a gel with gradual change of thickness. Pouring liquid agar on a tilted dish resulted in a  
215 gel with a spatial gradient of thickness: on this substrate, the swelling front advanced faster on

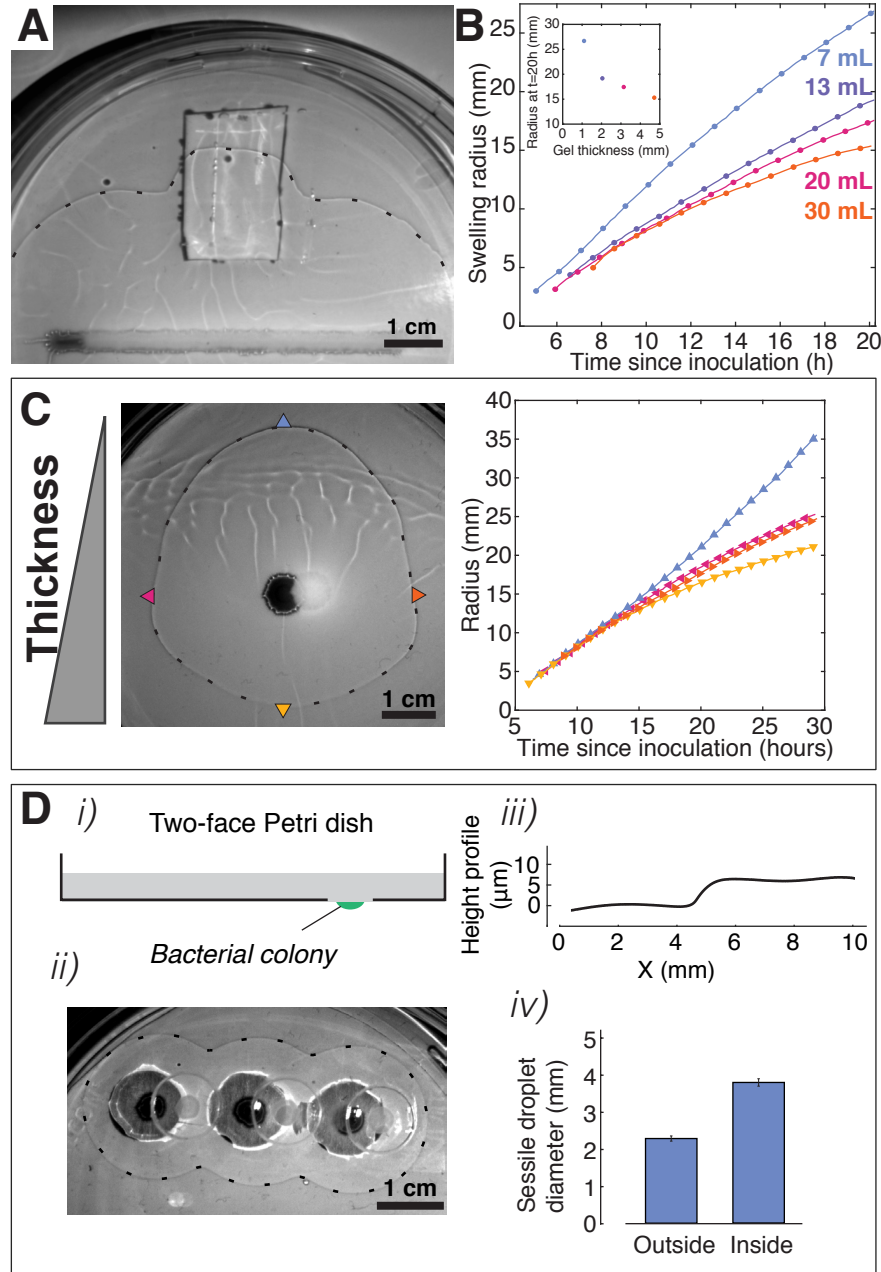


Figure 2: A: Snapshot of the swelling front on a plate with an obstacle. The non-motile colony, inoculated along a line, is visible near the bottom of the image. B: Positions of the swelling front as a function of time, for four plates with different thicknesses of gel. C: Left: Snapshot of the swelling front advancing on a tilted gel. Right: Positions of the swelling front as a function of time, for 4 locations depicted with arrowheads (top, bottom, left, and right). D: Two-face Petri dish confirms rhamnolipids spread through the gel. i) Schematic of a two-face Petri dish. ii) Shadowgraph of the swelling front emerging from three colonies, located on the other side of the gel. iii) Height profile obtained from optical profilometry. iv) Sessile droplet experiment confirms an significant difference in wetting property on either side of the swelling front. Error bars are standard deviation.

216 the thinning side, slower on the thickening side, and at intermediate speed on the transverse  
217 directions (Figure 2B). Colony did not swarm at all on plates lower than 7 mL. They gradually  
218 were larger and larger on thicker gels and the colony size was maximal on plates of the nominal  
219 volume (20 mL).

220 To further demonstrate transport of rhamnolipids through gels, I designed a "two-face" Petri  
221 dish. I inoculated bacteria on the lower side of the dish and a swelling front was observed on the  
222 upper side. The upper surface was characterized with shadowgraphy, profilometry, and sessile  
223 droplets (Figure 2D). These measurements confirmed that a rhamnolipid-induced swelling front  
224 propagated to the upper surface, even though rhamnolipids were secreted from the lower surface.

### 225 *Rhamnolipids enable surface motility at the single-cell level*

226 Rhamnolipids, transported within the gel, are required for the colony to spread at the surface of  
227 the gel. To better understand the interplay between bulk transport of rhamnolipids and surface  
228 motility, I used *rhlA*<sup>-</sup> mutant, which does not secrete rhamnolipids but is motile, as a sensor of  
229 ability to move on the gel as a function of presence of rhamnolipids. A wild-type colony was  
230 grown on agar gel and a small amount of planktonic *rhlA*<sup>-</sup> cells were seeded on the naked gel. In-  
231 dividual cells were found to be initially mostly non-motile. Motility was detected only in denser  
232 areas. The passage of the swelling front dramatically perturbed spatial organization of the cells  
233 (Figure 3A and Movie S3), and hampered direct comparison before/after. In particular, following  
234 individual cells was impossible. Instead, motility was assessed by coarse-grained image analysis  
235 (see Methods). The motility-density dependence was quantified and plotted against time (Figure  
236 3B-C). Even though cells gradually became more motile with time, incoming rhamnolipids sub-  
237 stantially increased cell motility, at all densities (Movie S4). Therefore, rhamnolipids are used by  
238 bacteria to alter their physical environment over large distances and enable surface motility.

### 239 *Swarming rescue experiments confirm rhamnolipids diffuse across the biogel*

240 This microscopic-scale rescue of motility *rhlA*<sup>-</sup> mutants inspired me to test if such distant rescue  
241 could occur at a macroscopic scale. A plate was inoculated with wild-type cells on one side, and

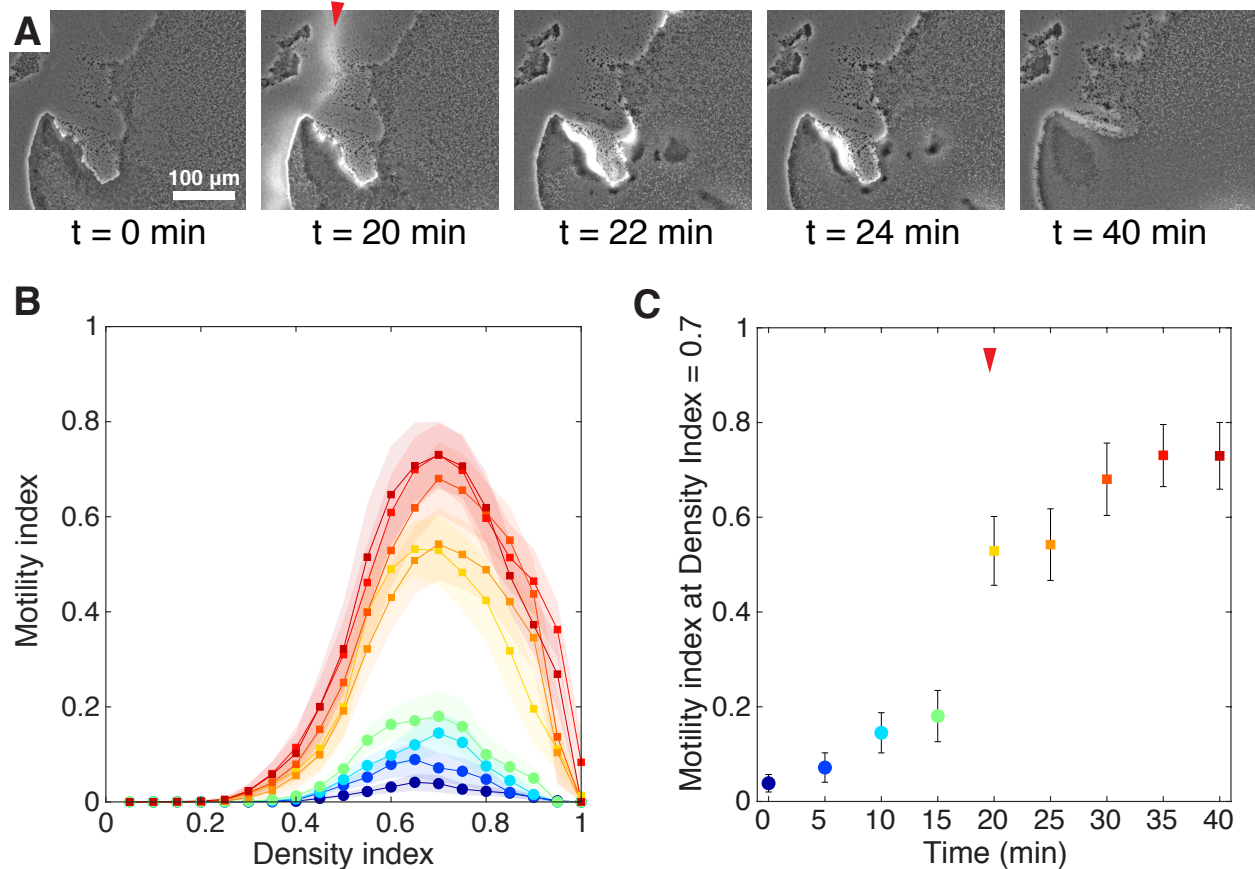


Figure 3: A: Snapshots of micrographs showing *rhlA*<sup>-</sup> cells before and after the swelling front passed through. A red arrowhead depicts the swelling front, visible as a white halo in phase contrast imaging, and moving from the left to the right of the field of view. B: Motility-density analysis reveals rhamnolipids greatly facilitate single-cell motility. Color code is defined in panel C (one curve every 5 minutes). Shading represents standard deviations. C: The effect of rhamnolipids on motility is abrupt, and corresponds to the passage of the swelling front (depicted by the red arrowhead). Error bars represent standard deviations.

242 with *rhlA*<sup>-</sup> cells on the other side. As already showed in Figure 1, the wild-type colony secretes  
243 rhamnolipids (inducing a swelling front) and swarms into a branched shape. The *rhlA*<sup>-</sup> colony  
244 does not secrete rhamnolipids and does not swarm. However, wild-type colony spreading closely  
245 follows the swelling front. To avoid the *rhlA*<sup>-</sup> colony from being reached by the expanding wild-  
246 type colony before it started swarming, I turned into a mutant over-producer of rhamnolipids:  
247 *rhlA*<sup>-</sup> *pBAD-RhlAB*, whose rhamnolipid promoter expression is induced by a chemical cue, L-  
248 arabinose. The *rhlA*<sup>-</sup> *pBAD-RhlAB* colony dedicates a large part of its metabolism to rhamnolipid  
249 secretion rather than cell proliferation, which yields to a faster swelling front and a slower colony  
250 spreading. As shown on Figure 4A (and Movie S5), *rhlA*<sup>-</sup> colonies started swarming a few  
251 hours after the swelling front reached it. Interestingly, the *rhlA*<sup>-</sup> colonies did not spread radially,  
252 but formed tendrils, whose size is comparable to wild-type colony branches. These tendrils  
253 swarmed outward, following the direction of rhamnolipids propagation. These observations  
254 are in agreement with the surface tension induced spreading mechanism, where a gradient of  
255 surfactants concentration at the colony surface induce a Marangoni stress [40].

256 I reproduced the rescue experiment on a two-face Petri dish, with the over-producing colony  
257 (*rhlA*<sup>-</sup> *pBAD-RhlAB*) on one side and *rhlA*<sup>-</sup> on the other side (Figure 4B, Movie S5). Here again,  
258 the *rhlA*<sup>-</sup> colonies did not spread radially, but formed a tendril spreading in the direction of  
259 rhamnolipid propagation. This confirms rhamnolipids imbibe the whole gel, physically alter the  
260 gel over large distance, and generate a gradient of concentration on the opposite surface, which  
261 yield to colony branching following Marangoni effect.

### 262 *Physical alteration of the gel by rhamnolipids correlates with colony shape*

263 Since *P. aeruginosa* is capable to alter physical properties of its environment over long distances,  
264 I wanted to verify whether this would hold true for a range of environments. I used agar gels of  
265 various agar concentrations (0.4%, 0.5%, 0.6%, and 0.7%) to simulate environments of different  
266 physical properties. Agar gel elastic modulus and pore size were previously characterized and  
267 they were found to be highly dependent on agar concentration. From the literature, pore size  
268 varies from 400 nm at 0.4% to 100 nm at 0.7% [48, 49]; elastic modulus varies from 4 kPa at 0.4%

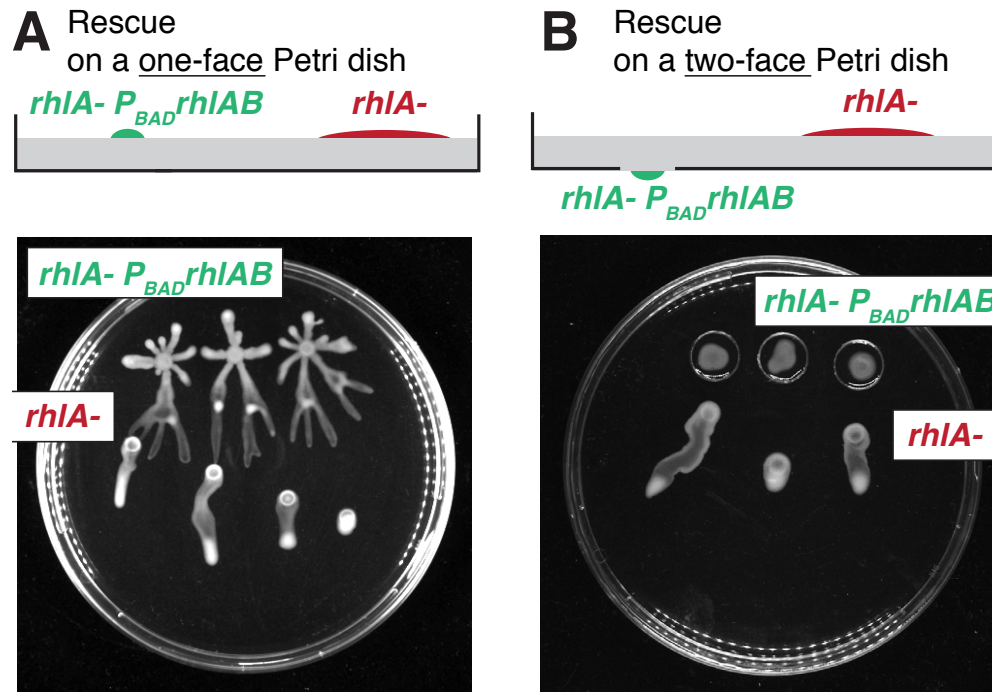


Figure 4: Swarming rescue experiments. A: On one-face Petri dish, *rhIA*<sup>-</sup> *pBAD-RhlAB* and *rhIA*<sup>-</sup> colonies are grown on the same side. B: On two-face Petri dish, *rhIA*<sup>-</sup> *pBAD-RhlAB* are grown on one side (within the small hole) and *rhIA*<sup>-</sup> are grown on the opposite side. Control experiment results (with *rhIA*<sup>-</sup> instead of *rhIA*<sup>-</sup> *pBAD-RhlAB*) are provided in Supplementary Figure S3. Snapshots are taken 18 hours after inoculation. Timelapse videos of the rescue experiments are available in Movie S5.

269 to 18 kPa at 0.7% [50, 51]. (Most studies focused on agarose, a polysaccharide isolated from agar,  
270 but with comparable mechanical properties; rheological measurements are difficult to perform  
271 on these soft gels, and those figures must be taken with a grain of salt.)

272 I grew *P. aeruginosa* on plates at the four agar concentrations and confirmed a result already  
273 described: swarming colony morphogenesis is highly dependent on the gel properties (Figure  
274 5A). At low concentration (0.4%), the colony was smaller and more circular than the branch  
275 colony formed at 0.5%. At 0.6%, the colony was still branched but smaller than 0.5% colony.  
276 The 0.7% colony did not spread at all. Following the same trend, macroscopic swarming rescue  
277 on two-face Petri dished occurred similarly at 0.4% and 0.5% (once again forming tendrils, in  
278 agreement with Marangoni mechanisms for surface tension induced spreading), little spreading  
279 was visible at 0.6%, and no spreading at all at 0.7% (Figure 5B). In parallel, I characterized the  
280 gel and its alteration by secreted rhamnolipids, for the four agar concentrations.

281 First, I reproduced the sessile droplet experiment as in Figure 1D. Footprint diameters in-  
282 creased with gel concentration when droplets were deposited on the raw gel surface (outside the  
283 rhamnolipid imbibed area), from  $1.77 \pm 0.13$  mm for 0.4% to  $2.41 \pm 0.10$  mm for 0.7% (Figure  
284 5C). In contrast, when droplets were deposited inside the rhamnolipids-imbibed area, footprint  
285 diameters were overall much greater and independent of agar concentrations. They were about  
286  $3.86 (\pm 0.27)$  mm for all conditions, as if rhamnolipids equalized the wetting properties of the  
287 imbibed gels.

288 Second, I measured the swelling front height profiles generated by rhamnolipid imbibition  
289 (Figure 5D). I observed a strong influence of agar concentration: the swelling front jump (mea-  
290 sured 1 mm away from the front, see details in Methods) was  $27.4 \pm 4.2$   $\mu$ m for 0.4% and gradually  
291 decreased for larger agar concentrations ( $3.9 \pm 1.8$   $\mu$ m for 0.7%). This trend was confirmed by  
292 shadowgraphy, a contrast imaging method that relies on non-uniformities deviating light rays:  
293 the front on a 0.4% gel yielded to a strongly contrasted black line, whereas the front on a 0.7%  
294 gel was nearly not visible.

295 Third, I located the position of the swelling front as a function of time, on two-face Petri  
296 dishes. An *rhlA*<sup>-</sup> *pBAD-RhlAB* colony was seeded on the small aperture on the opposite side,

297 in order to limit the spatial expansion of the rhamnolipid source and to allow for comparison  
298 of swelling front advancing speeds across agar concentrations without having to control for the  
299 source colony size. The position of the swelling front followed a power law  $r = t^\alpha$  with  $\alpha$  ranging  
300 between 0.4 and 0.6 (Figure 5D, inset), in agreement with imbibition processes [52]. However,  
301 a reproducible estimation of the exponent was difficult, considering the day-to-day variability of  
302 agar gel preparation previously described [53, 54, 55]. I turned to a simpler and more robust  
303 quantification: the position of the front 15 hours after inoculation. Using this measure, I found  
304 that the swelling front advanced significantly faster in low concentration agar gels compared to  
305 high concentration agar gels (Figure 5E).

306 Taken together, these results demonstrate that swarming colony morphogenesis correlates  
307 with the long distance physical alteration of the gel, across a range of agar concentrations.

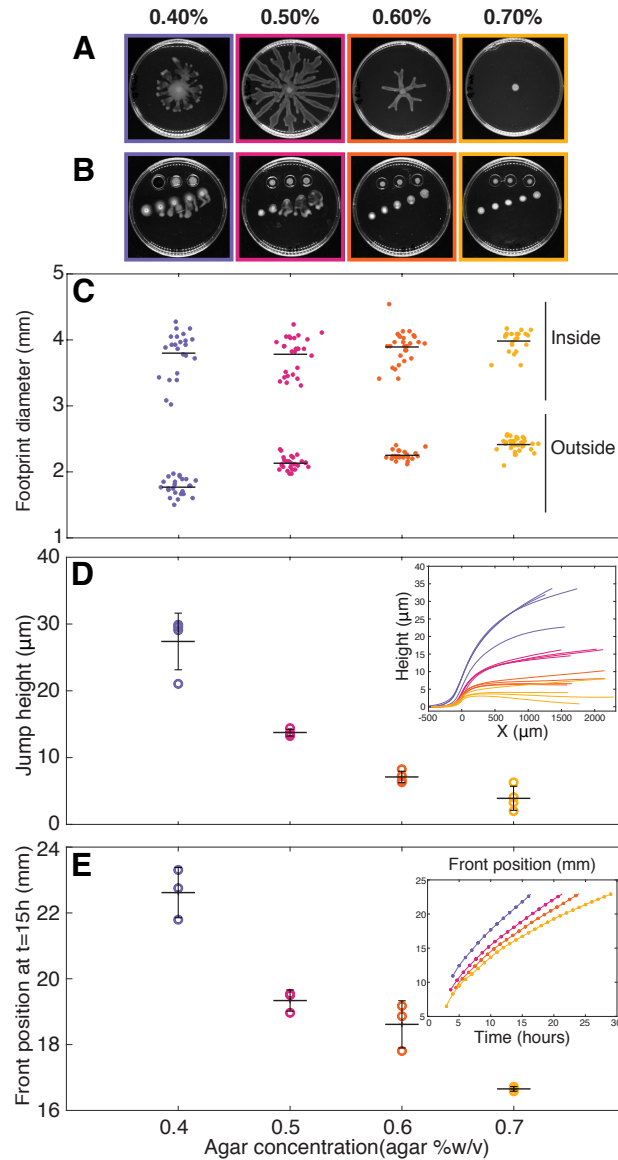


Figure 5: Physical alteration of the gel occurs across a range of agar concentration. A: Snapshots of *P. aeruginosa* swarming colonies, 22 hours after inoculation. Each snapshot is surrounded by a square whose color consistently represents the agar concentration across panels. B: Snapshots of macroscopic rescue experiments, 22 hours after inoculation. (Note one agar patch fell from the two-face Petri dish on the 0.4% plate, just before image acquisition.) C: Footprint diameters for sessile droplet experiments. Droplets were deposited within the rhamnolipid-imbibed area (denoted "Inside") or outside the swelling front (denoted "Outside"). Data points positions were randomized on the horizontal axis for better visualization. Data points originates from 2 biological replicates. D: Jump height measured 1 mm from the swelling front. Inset: Height profiles obtained by optical interferometry. E: Position of the swelling front 15 hours after inoculation. Data points originates from 3 technical replicates. Inset: Time evolution of the front position, from one replicate. For all panels, horizontal bars are dataset averages and vertical bars are standard deviations.

308

## Discussion

309 Self-produced surfactants play an critical role in a many bacterial genera. For example, the  
310 swarming of *Rhizobium etli* [56], *Serratia marcescens* [57], *Bacillus subtilis* [58], and *P. aeruginosa* [30]  
311 were shown to be linked to the presence of biosurfactants. Here, I documented that rhamnolipids,  
312 secreted by *P. aeruginosa*, physically modify the agar gel by inducing a gel swelling. The swelling  
313 front displays a maximum angle of  $3^\circ$  that is sufficient to make the edge visible to the naked eye  
314 and by shadowgraphy. Previous work had already noted a change of the surface visual aspect.  
315 Those studies used terms like "zone of fluid", "zone of liquid" [30], or "ring of biosurfactants"  
316 [31] to describe this modified surface state, but my findings show those views were incomplete.  
317 Further investigation will be necessary to understand the swelling mechanism, which might  
318 involve complex interplay between gel pores, osmolarity, hydrophobic interactions, etc., and  
319 goes beyond the scope of this study.

320 Additionally, I demonstrated that transport of rhamnolipids is not restricted to the surface  
321 of the agar gel. On the contrary, rhamnolipids imbibe the whole thickness of the gel. A direct  
322 consequence of the transport in volume is that spreading speed depends on the local section of  
323 the gel, with faster spreading on thinner gels. The modulation of the swelling front traveling  
324 speed is likely to be conflated with resource availability: a thinner gel contains less nutrient,  
325 yields to a smaller colony, and is expected to produce to a slower swelling front. Experimental  
326 data goes in the opposite direction: thinner gels yields to faster, not slower, swelling front. In-  
327 terestingly, colonies do not spread faster on thinner gel. This highlights the complex interplay  
328 between resources availability, rhamnolipids spatial distribution, and swarming motility [31, 33].

329 The swelling front advancing speed, typically 1 mm/h, is substantially lower than the spread-  
330 ing dynamics of surfactants on liquid films (typically 1 mm/s [37]). It resembles precursor front  
331 in fluid imbibition dynamics of porous materials, which can be interpreted as non-Fickian trans-  
332 port in a Darcy flow [52]. Moreover, the deformation of the agar gel is likely to be coupled to  
333 the effective diffusivity of rhamnolipids through the gel. Since rhamnolipids are capable to reach  
334 the opposite surface, one could assume, in first approximation, a uniform concentration profile

335 across the gel thickness. Yet, agar gel is a physically-crosslinked hydrogel, and the physico-  
336 chemistry of its interaction with surfactants could lead to a non-uniform profile of concentration  
337 [47, 59]. Colony branching in two-face rescue experiments confirms that bulk gel imbibition  
338 generates a lateral gradient of surfactant concentration that could potentially interact with the  
339 spreading colony itself.

340 Alteration of the biotic or abiotic environment by living organisms have the potential to  
341 modulate motility and dispersal mechanics. Secreted metabolites can act as chemoattractants [60,  
342 61], trigger quorum sensing [62], participate in self-organization in stigmergic behavior [63, 64],  
343 and control single-cell motility [65]. These mechanisms rely on release of diffusible molecules,  
344 or local deposition of non-diffusible signals. Here, I evidenced a mechanism where bacteria alter  
345 their physical world on a lengthscale substantially larger than their own size. I confirmed this  
346 effect holds true across a range of agar concentration. It would be interesting to test other biogel  
347 materials [66], especially those with biomedical implications, such as mucus [67, 68]. Moreover,  
348 rhamnolipids are shown to be involved in many killing processes (towards other bacteria [69],  
349 fungus [70], immune cells [71], or higher organisms [72, 73]): understanding how this killing  
350 agent is transported through complex media is of critical importance.

351 This complex interplay between surfactants secretion, biogel properties alteration and bacte-  
352 rial motility is a unique example of the capacity of bacteria to change the mechanical properties  
353 of the world around them, and ultimately, to interact with their distant peers [74].

## 354 **Acknowledgments**

355 I thank members of the Laboratoire Jean Perrin for fruitful discussions. I am grateful to Françoise  
356 Brochard-Wyart for pointing me to the reference [52]. This project has received financial support  
357 from the CNRS through the MITI interdisciplinary program, from the Alliance Sorbonne Univer-  
358 sity through the Emergence program, and from the ANR (ANR-21-CE30-0025).

## References

- 359
- 360 [1] Kai Papenfort and Bonnie L Bassler. Quorum sensing signal–response systems in gram-  
361 negative bacteria. *Nature Reviews Microbiology*, 14(9):576–588, 2016.
- 362 [2] Despoina AI Mavridou, Diego Gonzalez, Wook Kim, Stuart A West, and Kevin R Foster. Bac-  
363 teria use collective behavior to generate diverse combat strategies. *Current Biology*, 28(3):345–  
364 355, 2018.
- 365 [3] Christoph Ratzke and Jeff Gore. Modifying and reacting to the environmental ph can drive  
366 bacterial interactions. *PLoS biology*, 16(3):e2004248, 2018.
- 367 [4] Alexandre Persat, Carey D Nadell, Minyoung Kevin Kim, Francois Ingremeau, Albert Sirya-  
368 porn, Knut Drescher, Ned S Wingreen, Bonnie L Bassler, Zemer Gitai, and Howard A Stone.  
369 The mechanical world of bacteria. *Cell*, 161(5):988–997, 2015.
- 370 [5] Veysel Berk, Jiunn CN Fong, Graham T Dempsey, Omer N Develioglu, Xiaowei Zhuang, Jan  
371 Liphardt, Fitnat H Yildiz, and Steven Chu. Molecular architecture and assembly principles  
372 of vibrio cholerae biofilms. *Science*, 337(6091):236–239, 2012.
- 373 [6] Su Chuen Chew, Binu Kundukad, Thomas Seviour, Johan RC Van der Maarel, Liang Yang,  
374 Scott A Rice, Patrick Doyle, and Staffan Kjelleberg. Dynamic remodeling of microbial  
375 biofilms by functionally distinct exopolysaccharides. *MBio*, 5(4):e01536–14, 2014.
- 376 [7] Carolina Tropini. How the physical environment shapes the microbiota. *Msystems*,  
377 6(4):e00675–21, 2021.
- 378 [8] Navish Wadhwa and Howard C Berg. Bacterial motility: machinery and mechanisms. *Nature*  
379 *Reviews Microbiology*, pages 1–13, 2021.
- 380 [9] Derek Greenfield, Ann L McEvoy, Hari Shroff, Gavin E Crooks, Ned S Wingreen, Eric Betzig,  
381 and Jan Liphardt. Self-organization of the escherichia coli chemotaxis network imaged with  
382 super-resolution light microscopy. *PLoS biology*, 7(6):e1000137, 2009.

- 383 [10] Remy Colin, Bin Ni, Leanid Laganenka, and Victor Sourjik. Multiple functions of flagellar  
384 motility and chemotaxis in bacterial physiology. *FEMS Microbiology Reviews*, 45(6):fuab038,  
385 2021.
- 386 [11] OK Mirzoeva, RN Grishanin, and PC Calder. Antimicrobial action of propolis and some  
387 of its components: the effects on growth, membrane potential and motility of bacteria.  
388 *Microbiological research*, 152(3):239–246, 1997.
- 389 [12] Michael Baym, Tami D Lieberman, Eric D Kelsic, Remy Chait, Rotem Gross, Idan Yelin,  
390 and Roy Kishony. Spatiotemporal microbial evolution on antibiotic landscapes. *Science*,  
391 353(6304):1147–1151, 2016.
- 392 [13] Ruth Daniels, Jos Vanderleyden, and Jan Michiels. Quorum sensing and swarming migra-  
393 tion in bacteria. *FEMS microbiology reviews*, 28(3):261–289, 2004.
- 394 [14] Nachiket G Kamatkar and Joshua D Shrout. Surface hardness impairment of quorum sens-  
395 ing and swarming for pseudomonas aeruginosa. *PloS one*, 6(6):e20888, 2011.
- 396 [15] Hannah Jeckel, Eric Jelli, Raimo Hartmann, Praveen K Singh, Rachel Mok, Jan Frederik Tetz,  
397 Lucia Vidakovic, Bruno Eckhardt, Jörn Dunkel, and Knut Drescher. Learning the space-time  
398 phase diagram of bacterial swarm expansion. *Proceedings of the National Academy of Sciences*,  
399 116(5):1489–1494, 2019.
- 400 [16] Divakar Badal, Abhijith Vimal Jayarani, Mohammad Ameen Kollaran, Deep Prakash, Mon-  
401 isha P, Varsha Singh, and Joanna B. Goldberg. Foraging signals promote swarming in starv-  
402 ing pseudomonas aeruginosa. *mBio*, 0(0):e02033–21, 2021.
- 403 [17] Hilary Monaco, Kevin S Liu, Tiago Sereno, Maxime Deforet, Bradford P Taylor, Yanyan  
404 Chen, Caleb C Reagor, and Joao B Xavier. Spatial-temporal dynamics of a microbial cooper-  
405 ative behavior resistant to cheating. *Nature communications*, 13(1):1–11, 2022.
- 406 [18] Gabriel E Dilanji, Max Teplitski, and Stephen J Hagen. Entropy-driven motility of *Sinorhi-*  
407 *zobium meliloti* on a semi-solid surface. *Proceedings of the Royal Society B: Biological Sciences*,  
408 281(1784):20132575, 2014.

- 409 [19] Agnese Seminara, Thomas E Angelini, James N Wilking, Hera Vlamakis, Senan Ebrahim,  
410 Roberto Kolter, David A Weitz, and Michael P Brenner. Osmotic spreading of bacillus  
411 subtilis biofilms driven by an extracellular matrix. *Proceedings of the National Academy of*  
412 *Sciences*, 109(4):1116–1121, 2012.
- 413 [20] Alexander Yang, Wai Shing Tang, Tieyan Si, and Jay X. Tang. Influence of physical effects  
414 on the swarming motility of pseudomonas aeruginosa. *Biophysical Journal*, 112(7):1462–1471,  
415 2017.
- 416 [21] Hui Ma, Jordan Bell, Weijie Chen, Sridhar Mani, and Jay X Tang. An expanding bacterial  
417 colony forms a depletion zone with growing droplets. *Soft Matter*, 17(8):2315–2326, 2021.
- 418 [22] Ben Rhodeland, Kentaro Hoeger, and Tristan Ursell. Bacterial surface motility is mod-  
419 ulated by colony-scale flow and granular jamming. *Journal of the Royal Society Interface*,  
420 17(167):20200147, 2020.
- 421 [23] Siddarth Srinivasan, C Nadir Kaplan, and L Mahadevan. A multiphase theory for spreading  
422 microbial swarms and films. *Elife*, 8:e42697, 2019.
- 423 [24] Jing Yan, Carey D Nadell, Howard A Stone, Ned S Wingreen, and Bonnie L Bassler.  
424 Extracellular-matrix-mediated osmotic pressure drives vibrio cholerae biofilm expansion  
425 and cheater exclusion. *Nature communications*, 8(1):1–11, 2017.
- 426 [25] Priyanka Thakur, Neeraj K Saini, Vijay Kumar Thakur, Vijai Kumar Gupta, Reena V Saini,  
427 and Adesh K Saini. Rhamnolipid the glycolipid biosurfactant: Emerging trends and promis-  
428 ing strategies in the field of biotechnology and biomedicine. *Microbial Cell Factories*, 20(1):1–  
429 15, 2021.
- 430 [26] A Varvaresou and K Iakovou. Biosurfactants in cosmetics and biopharmaceuticals. *Letters*  
431 *in applied microbiology*, 61(3):214–223, 2015.
- 432 [27] Eduardo J Gudiña, Ana I Rodrigues, Eliana Alves, M Rosário Domingues, José A Teix-  
433 eira, and Lúgia R Rodrigues. Bioconversion of agro-industrial by-products in rhamnolipids

- 434 toward applications in enhanced oil recovery and bioremediation. *Bioresource technology*,  
435 177:87–93, 2015.
- 436 [28] Matthew F Copeland and Douglas B Weibel. Bacterial swarming: a model system for study-  
437 ing dynamic self-assembly. *Soft matter*, 5(6):1174–1187, 2009.
- 438 [29] Daniel B Kearns. A field guide to bacterial swarming motility. *Nature Reviews Microbiology*,  
439 8(9):634–644, 2010.
- 440 [30] Nicky C. Caiazza, Robert M. Q. Shanks, and G. A. O’Toole. Rhamnolipids modulate swarm-  
441 ing motility patterns of *Pseudomonas aeruginosa*. *Journal of Bacteriology*, 187(21):7351–  
442 7361, 2005.
- 443 [31] Joao B Xavier, Wook Kim, and Kevin R Foster. A molecular mechanism that stabilizes  
444 cooperative secretions in *Pseudomonas aeruginosa*. *Molecular microbiology*, 79(1):166–179,  
445 2011.
- 446 [32] Judy Q Yang, Joseph E Sanfilippo, Niki Abbasi, Zemer Gitai, Bonnie L Bassler, and  
447 Howard A Stone. Evidence for biosurfactant-induced flow in corners and bacterial  
448 spreading in unsaturated porous media. *Proceedings of the National Academy of Sciences*,  
449 118(38):e2111060118, 2021.
- 450 [33] Kerry E Boyle, Hilary Monaco, Dave van Ditmarsch, Maxime Deforet, and Joao B Xavier.  
451 Integration of metabolic and quorum sensing signals governing the decision to cooperate in  
452 a bacterial social trait. *PLoS computational biology*, 11(6):e1004279, 2015.
- 453 [34] Theresa Hölscher and Ákos T Kovács. Sliding on the surface: bacterial spreading without  
454 an active motor. *Environmental Microbiology*, 19(7):2537–2545, 2017.
- 455 [35] Julien Tremblay, Anne-Pascale Richardson, François Lépine, and Eric Déziel. Self-produced  
456 extracellular stimuli modulate the *Pseudomonas aeruginosa* swarming motility behaviour.  
457 *Environmental Microbiology*, 9(10):2622–2630, 2007.

- 458 [36] Sina Rütschlin and Thomas Böttcher. Inhibitors of bacterial swarming behavior. *Chemistry–A*  
459 *European Journal*, 26(5):964–979, 2020.
- 460 [37] Omar K Matar and Sandra M Troian. The development of transient fingering patterns during  
461 the spreading of surfactant coated films. *Physics of Fluids*, 11(11):3232–3246, 1999.
- 462 [38] Omar K Matar and Richard V Craster. Dynamics of surfactant-assisted spreading. *Soft*  
463 *Matter*, 5(20):3801–3809, 2009.
- 464 [39] Maarten Fauvart, P Phillips, D Bachaspatimayum, Natalie Verstraeten, Jan Fransaer, Jan  
465 Michiels, and Jan Vermant. Surface tension gradient control of bacterial swarming in  
466 colonies of pseudomonas aeruginosa. *Soft Matter*, 8(1):70–76, 2012.
- 467 [40] Sarah Trinschek, Karin John, and Uwe Thiele. Modelling of surfactant-driven front instabil-  
468 ities in spreading bacterial colonies. *Soft Matter*, 14(22):4464–4476, 2018.
- 469 [41] Ahmad Mohammad Abdel-Mawgoud, Mohammad Mabrouk Aboulwafa, and Nadia Abdel-  
470 Haleem Hassouna. Characterization of rhamnolipid produced by pseudomonas aeruginosa  
471 isolate bs20. *Applied biochemistry and biotechnology*, 157(2):329–345, 2009.
- 472 [42] Azeem Bibi, Sadiq-ur Rehman, Rashida Faiz, Tasleem Akhtar, Mohsan Nawaz, and Saira  
473 Bibi. Effect of surfactants on swelling capacity and kinetics of alginate-chitosan/cnts hydro-  
474 gel. *Materials Research Express*, 6(8):085065, 2019.
- 475 [43] Siyuan Li, Mengxue Zhang, and Bryan D Vogt. Delayed swelling and dissolution of hy-  
476 drophobically associated hydrogel coatings by dilute aqueous surfactants. *ACS Applied*  
477 *Polymer Materials*, 4(1):250–259, 2021.
- 478 [44] Gary S Settles. *Schlieren and shadowgraph techniques: visualizing phenomena in transparent media*.  
479 Springer Science & Business Media, 2001.
- 480 [45] Merced Gutierrez, Mun Hwan Choi, Baoxia Tian, Ju Xu, Jong Kook Rho, Myeong Ok Kim,  
481 You-Hee Cho, and Sung Chul Yoon. Simultaneous inhibition of rhamnolipid and poly-

- 482 hydroxyalkanoic acid synthesis and biofilm formation in *pseudomonas aeruginosa* by 2-  
483 bromoalkanoic acids: Effect of inhibitor alkyl-chain-length. *PLOS ONE*, 8(9):1–11, 09 2013.
- 484 [46] Wulin Teo, Andrew V. Caprariello, Megan L. Morgan, Antonio Luchicchi, Geert J. Schenk,  
485 Jeffrey T. Joseph, Jeroen J. G. Geurts, and Peter K. Stys. Nile red fluorescence spectroscopy  
486 reports early physicochemical changes in myelin with high sensitivity. *Proceedings of the*  
487 *National Academy of Sciences*, 118(8):e2016897118, 2021.
- 488 [47] Mehdi Banaha, Adrian Daerr, and Laurent Limat. Spreading of liquid drops on agar gels.  
489 *The European Physical Journal Special Topics*, 166(1):185–188, 2009.
- 490 [48] Janaky Narayanan, Jun-Ying Xiong, and Xiang-Yang Liu. Determination of agarose gel pore  
491 size: Absorbance measurements vis a vis other techniques. In *Journal of Physics: Conference*  
492 *Series*, volume 28, page 017. IOP Publishing, 2006.
- 493 [49] Nicholas L Cuccia, Suraj Pothineni, Brady Wu, Joshua Méndez Harper, and Justin C Bur-  
494 ton. Pore-size dependence and slow relaxation of hydrogel friction on smooth surfaces.  
495 *Proceedings of the National Academy of Sciences*, 117(21):11247–11256, 2020.
- 496 [50] Jean-Michel Guenet and Cyrille Rochas. Agarose sols and gels revisited. In *Macromolecular*  
497 *symposia*, volume 242, pages 65–70. Wiley Online Library, 2006.
- 498 [51] Bosi Mao, Thibaut Divoux, and Patrick Snabre. Normal force controlled rheology applied  
499 to agar gelation. *Journal of Rheology*, 60(3):473–489, 2016.
- 500 [52] Eduardo N de Azevedo, Lars R Alme, M Engelsberg, Jon Otto Fossum, and Paul Dom-  
501 mersnes. Fluid imbibition in paper fibers: Precursor front. *Physical Review E*, 78(6):066317,  
502 2008.
- 503 [53] Julien Tremblay and Eric Déziel. Improving the reproducibility of *pseudomonas aeruginosa*  
504 swarming motility assays. *Journal of basic microbiology*, 48(6):509–515, 2008.

- 505 [54] Dae-Gon Ha, Sherry L Kuchma, and George A O'Toole. Plate-based assay for swarming  
506 motility in *Pseudomonas aeruginosa*. In *Pseudomonas methods and protocols*, pages 67–72.  
507 Springer, 2014.
- 508 [55] Melanie M Pearson. Methods for studying swarming and swimming motility. In *Proteus*  
509 *mirabilis*, pages 15–25. Springer, 2019.
- 510 [56] Ruth Daniels, Sven Reynaert, Hans Hoekstra, Christel Verreth, Joost Janssens, Kristien  
511 Braeken, Maarten Fauvart, Serge Beullens, Christophe Heusdens, Ivo Lambrichts, et al. Quo-  
512 rum signal molecules as biosurfactants affecting swarming in *rhizobium etli*. *Proceedings of*  
513 *the National Academy of Sciences*, 103(40):14965–14970, 2006.
- 514 [57] Sunny Ang, Yu-Tze Horng, Jwu-Ching Shu, Po-Chi Soo, Jia-Hurng Liu, Wen-Chin Yi, Hsin-  
515 Chih Lai, Kwen-Tay Luh, Shen-Wu Ho, and Simon Swift. The role of *rsma* in the regulation  
516 of swarming motility in *serratia marcescens*. *Journal of biomedical science*, 8(2):160–169, 2001.
- 517 [58] Thomas E Angelini, Marcus Roper, Roberto Kolter, David A Weitz, and Michael P Brenner.  
518 *Bacillus subtilis* spreads by surfing on waves of surfactant. *Proceedings of the National Academy*  
519 *of Sciences*, 106(43):18109–18113, 2009.
- 520 [59] Shilpi Boral, Anita Saxena, and HB Bohidar. Syneresis in agar hydrogels. *International journal*  
521 *of biological macromolecules*, 46(2):232–236, 2010.
- 522 [60] Evanthia T Roussos, John S Condeelis, and Antonia Patsialou. Chemotaxis in cancer. *Nature*  
523 *Reviews Cancer*, 11(8):573–587, 2011.
- 524 [61] Remy Colin and Victor Sourjik. Emergent properties of bacterial chemotaxis pathway. *Cur-*  
525 *rent opinion in microbiology*, 39:24–33, 2017.
- 526 [62] Christopher M Waters, Bonnie L Bassler, et al. Quorum sensing: cell-to-cell communication  
527 in bacteria. *Annual review of cell and developmental biology*, 21(1):319–346, 2005.
- 528 [63] Guy Theraulaz and Eric Bonabeau. A brief history of stigmergy. *Artificial life*, 5(2):97–116,  
529 1999.

- 530 [64] Joseph D'alessandro, Victor Cellerin, Olivier Benichou, René Marc Mège, Raphaël Voituriez,  
531 Benoît Ladoux, et al. Cell migration guided by long-lived spatial memory. *Nature Commu-*  
532 *nications*, 12(1):1–10, 2021.
- 533 [65] Esther Wershof, Danielle Park, Robert P Jenkins, David J Barry, Erik Sahai, and Paul A Bates.  
534 Matrix feedback enables diverse higher-order patterning of the extracellular matrix. *PLoS*  
535 *computational biology*, 15(10):e1007251, 2019.
- 536 [66] Charles D Morin and Eric Déziel. Use of alternative gelling agents reveals the role of rham-  
537 nolipids in pseudomonas aeruginosa surface motility. *Biomolecules*, 11(10):1468, 2021.
- 538 [67] Amy TY Yeung, Alicia Parayno, and Robert EW Hancock. Mucin promotes rapid surface  
539 motility in pseudomonas aeruginosa. *MBio*, 3(3):e00073–12, 2012.
- 540 [68] Tamara Rossy, Tania Distler, Joern Pezoldt, Jaemin Kim, Lorenzo Tala, Nikolaos Bouklas,  
541 Bart Deplancke, and Alexandre Persat. Pseudomonas aeruginosa contracts mucus to rapidly  
542 form biofilms in tissue-engineered human airways. *bioRxiv*, 2022.
- 543 [69] P Bharali, JP Saikia, A Ray, and BK Konwar. Rhamnolipid (rl) from pseudomonas aerugi-  
544 nosa obp1: a novel chemotaxis and antibacterial agent. *Colloids and Surfaces B: Biointerfaces*,  
545 103:502–509, 2013.
- 546 [70] Soroosh Soltani Dashtbozorg, Shida Miao, and Lu-Kwang Ju. Rhamnolipids as environ-  
547 mentally friendly biopesticide against plant pathogen phytophthora sojae. *Environmental*  
548 *Progress & Sustainable Energy*, 35(1):169–173, 2016.
- 549 [71] Peter Ø Jensen, Thomas Bjarnsholt, Richard Phipps, Thomas B Rasmussen, Henrik  
550 Calum, Lars Christoffersen, Claus Moser, Paul Williams, Tacjana Pressler, Michael Givskov,  
551 et al. Rapid necrotic killing of polymorphonuclear leukocytes is caused by quorum-  
552 sensing-controlled production of rhamnolipid by pseudomonas aeruginosa. *Microbiology*,  
553 153(5):1329–1338, 2007.
- 554 [72] Alexander Zaborin, Kathleen Romanowski, Svetlana Gerdes, Christopher Holbrook, Fran-  
555 cois Lepine, Jason Long, Valeriy Poroyko, Stephen P Diggle, Andreas Wilke, Karima

- 556 Righetti, et al. Red death in *Caenorhabditis elegans* caused by *Pseudomonas aeruginosa*  
557 pao1. *Proceedings of the National Academy of Sciences*, 106(15):6327–6332, 2009.
- 558 [73] Vinicius L Silva, Roberta B Lovaglio, Claudio J Von Zuben, and Jonas Contiero. Rhamno-  
559 lipids: solution against *Aedes aegypti*? *Frontiers in Microbiology*, 6:88, 2015.
- 560 [74] Sylvie Estrela, Eric Libby, Jeremy Van Cleve, Florence Débarre, Maxime Deforet, William R  
561 Harcombe, Jorge Peña, Sam P Brown, and Michael E Hochberg. Environmentally mediated  
562 social dilemmas. *Trends in ecology & evolution*, 34(1):6–18, 2019.